Quantitative Evaluation of Liver Function with Use of Gadoxetate Disodium–enhanced MR Imaging[1]

Akira Yamada, MD
Takeshi Hara, PhD
Feng Li, MD, PhD
Yasunari Fujinaga, MD, PhD
Kazuhiko Ueda, MD, PhD
Masumi Kadoya, MD, PhD
Kunio Doi, PhD

Purpose: To determine whether liver function correlating with indocyanine green (ICG) clearance could be estimated quantitatively from gadoxetate disodium–enhanced magnetic resonance (MR) images.

Materials and Methods: This retrospective study was approved by the institutional review board, and the requirement for informed consent was waived. Twenty-three consecutive patients who underwent an ICG clearance test and gadoxetate disodium–enhanced MR imaging with the same parameters as were used for a preoperative examination were chosen. The hepatocellular uptake index (HUI) from liver volume (V_L) and mean signal intensity of the liver on contrast-enhanced T1-weighted images with fat suppression (L_{20}) and mean signal intensity of the spleen on contrast-enhanced T1-weighted images with fat suppression (S_{20}) on 3D gradient-echo T1-weighted images with fat suppression obtained at 20 minutes after gadoxetate disodium (0.025 mmol per kilogram of body weight) administration was determined with the following equation: $V_L[(L_{20}/S_{20}) - 1]$. The correlation of the plasma disappearance rate of ICG (ICG-PDR) and various factors derived from MR imaging, including HUI, iron and fat deposition in the liver and spleen, and spleen volume (V_S), were evaluated with stepwise multiple regression analysis. The difference between the ratio of the remnant HUI to the HUI of the total liver (rHUI/HUI) and ratio of the liver remnant V_L to the total V_L (rV_L/V_L) was evaluated in four patients who had segmental heterogeneity of liver function.

Results: HUI and V_S were the factors significantly correlated with ICG-PDR ($R = 0.87$). The mean value and its 95% confidence interval were 0.18 and 0.01 to 0.34, respectively, for the following calculation: (rHUI/HUI) − (rV_L/V_L).

Conclusion: The liver function correlating with ICG-PDR can be estimated quantitatively from the signal intensities and the volumes of the liver and spleen on gadoxetate disodium–enhanced MR images, which may improve the estimation of segmental liver function.

[1] From the Department of Radiology, University of Chicago, Chicago, Ill (A.Y., T.H., F.L., K.D.); and Department of Radiology, Shinshu University School of Medicine, 3-1-1 Asahi, Matsumoto, Nagano 390-8621, Japan (A.Y., Y.F., K.U., M.K.). Received March 19, 2010; revision requested April 30; final revision received January 22, 2011; accepted March 2; final version accepted March 21. **Address correspondence to** A.Y. (e-mail: *a_yamada@shinshu-u.ac.jp*).

Quantitative evaluation of liver function is important not only for monitoring of that function, but also for preoperative assessment of the liver reserve (1). The ICG-PDR (abbreviations are defined in Table 1) has been regarded as a valuable tool for the quantitative assessment of liver function, because it is removed from the circulation exclusively by the liver (2). However, a reliable method for the quantitative anatomically based evaluation of liver function has not been established to date, to our knowledge.

Gadoxetate disodium (Primovist; Bayer Schering Pharma, Berlin, Germany) is a paramagnetic hepatobiliary contrast agent that can combine the features of extracellular agents with those of a hepatocellular contrast agent (3). The same transporting mechanisms (ie, the organic anion transporter) are considered to be responsible for uptake of gadoxetate disodium and ICG in hepatocytes (4,5); therefore, there is a possibility that gadoxetate disodium–enhanced MR imaging could be the basis of a useful method for quantitative evaluation of liver function similar to ICG clearance but with anatomic delineation of hepatic function (6–11).

The purpose of this study was to determine whether liver function correlating with ICG clearance could be estimated quantitatively from gadoxetate disodium–enhanced MR images.

Materials and Methods

Subjects

This retrospective study was approved by the institutional review boards of Shinshu University (Matsumoto, Japan) and the University of Chicago (Chicago, Ill), and the requirement for informed consent was waived.

There were 59 consecutive patients (49 men, 10 women; mean age, 69.9 years ± 9.0 [standard deviation]; range, 41–84 years) who underwent 3D GRE T1-weighted gadoxetate disodium–enhanced MR imaging and an ICG clearance test as a preoperative evaluation within 4 weeks from June 2008 to December 2009 in the record at the Shinshu University Hospital (Matsumoto, Japan). However, we selected only 23 patients for this study, as described below. Five patients (four men, one woman; mean age, 73.6 years; range, 57–87 years) were excluded because nonenhanced MR imaging was not performed. Twenty-one patients (19 men, two women; mean age, 68.9 years; range, 49–80 years) were excluded because the MR imaging parameters were different between nonenhanced and contrast material–enhanced MR imaging. Finally, 23 patients (17 men, six women; mean age, 70.0 years; range, 41–84 years) were selected for the evaluation because they were the largest population in this study of subjects whose MR imaging parameters (repetition time, echo time, flip angle) were the same at nonenhanced and contrast-enhanced 3D GRE MR imaging. There was no significant difference in the age and sex distribution between included and excluded patients. There were six patients without chronic hepatitis or liver cirrhosis, six patients with chronic hepatitis, and 11 patients with liver cirrhosis in this study group. No patient with renal dysfunction (serum creatinine level > 2.0 mg/dL [> 176.8 μmol/L]) was included in this study.

MR Imaging

Imaging of the entire liver and spleen was performed prior to and 20 minutes after intravenous administration of 0.025 mmol per kilogram body weight of gadoxetate disodium by using single-breath-hold 3D GRE or with fat suppression (repetition time msec/echo time msec, 3.5/1.42; flip angle, 15°) with an MR imaging system (Trio Tim; Siemens, Munich, Germany), an eight-channel phased-array body coil, and a parallel imaging technique (acceleration factor of two). Nonenhanced two-dimensional GRE T2*-weighted images (191–280/10 msec; flip angle, 20°) and nonenhanced two-dimensional dual-phase GRE T1-weighted images (106–165/1.23, 2.46; flip angle, 80°) were also obtained to evaluate iron and fat deposition in the liver and the spleen. The echo times in the dual-phase GRE sequence were determined according to actual magnetic field strength (2.8 T) of the MR imaging system.

Image Analysis

Two radiologists who were not authors and had 4 years and 3 years of experience in diagnostic imaging independently drew the outlines of the liver and spleen on every section of all MR images obtained, as listed above. In this procedure, MR images were presented on a Digital Imaging and Communications in Medicine viewer (Osirix; Pixmeo, Geneva,

Advance in Knowledge

- The liver function correlating with the ICG-PDR can be estimated quantitatively ($R = 0.87$) from the signal intensities and the volumes of the liver and the spleen on gadoxetate disodium–enhanced MR images.

Implications for Patient Care

- Our study results suggest that gadoxetate disodium–enhanced MR imaging of the liver may improve the early detection and treatment of liver diseases by allowing evaluation of anatomic and functional information of the liver in one examination.
- Gadoxetate disodium–enhanced MR imaging of the liver may allow quantitative estimation of segmental liver function.

Published online before print
10.1148/radiol.11100586 **Content code:** GI

Radiology 2011; 260:727–733

Author contributions:
Guarantors of integrity of entire study, K.U., M.K., K.D.; study concepts/study design or data acquisition or data analysis/interpretation, all authors; manuscript drafting or manuscript revision for important intellectual content, all authors; approval of final version of submitted manuscript, all authors; literature research, A.Y., Y.F., K.U., M.K., K.D.; clinical studies, A.Y., T.H., F.L., Y.F., K.U., M.K.; statistical analysis, A.Y., T.H., K.D.; and manuscript editing, A.Y., Y.F., K.U., M.K., K.D.

Potential conflicts of interest are listed at the end of this article.

Switzerland), and the outlines were drawn by using free-hand contours (Fig 1). The contrast-enhanced 3D GRE images were always presented first in order that observers could identify the liver parenchyma. The time limit for drawing outlines was not specified. In each patient, the V_L and V_S on contrast-enhanced images, the L_0 and S_0, the L_{in} and S_{in}, the L_{opp} and S_{opp}, the L_{T2*} and S_{T2*}, and the L_{20} and S_{20} were obtained within the volume included in the outlines. The average values for all parameters (V_L, V_S, L_0, S_0, L_{in}, S_{in}, L_{opp}, S_{opp}, L_{T2*}, S_{T2*}, L_{20}, and S_{20}) measured by the two radiologists were used for quantitative evaluation.

ICG Clearance Test

A dose of 0.5 mg/kg ICG was administered intravenously, and blood was withdrawn at 5-, 10-, and 15-minute intervals following ICG administration. ICG-PDR was determined with regression analysis (12). An ICG-PDR higher than 0.15 sec^{-1} can be considered to indicate normal liver function.

Feature Values Derived from Gadoxetate Disodium–enhanced MR Images

We introduced the feature value $V_L[(L_{20}/S_{20}) - 1]$, which may be called the HUI, as an index for the amount of gadoxetate disodium uptake into hepatocytes measured on gadoxetate disodium–enhanced MR images.

The feature values L_0/S_0, L_{T2*}/S_{T2*}, L_{opp}/L_{in}, S_{opp}/S_{in}, and V_S were evaluated to determine the degree of the difference in signal intensity between the liver and the spleen, the degree of the difference in iron deposition between the liver and the spleen (13), the degree of fat deposition in the liver (14), the degree of fat deposition in the spleen (14), and the degree of splenomegaly owing to portal hypertension, respectively.

Estimation of Segmental Liver Function in Patients with Segmental Heterogeneity of Liver Function

Conventionally, segmental liver function has been estimated by means of the ICG clearance test and volumetry (1). In this method, the segmental liver function could be estimated with the rV_L/V_L multiplied by ICG-PDR on the basis of the assumption that the liver function could be homogeneous; therefore, the ratio of the segmental liver function to the total liver function estimated with volumetry could be determined with rV_L/V_L. On the other hand, the segmental liver function could be estimated with the following equation: $rV_L[(rL_{20}/S_{20}) - 1]$, which may be called the rHUI as an index for the amount of gadoxetate disodium uptake into hepatocytes in rV_L measured on gadoxetate disodium–enhanced MR images, taking into account the heterogeneity of the liver function. The rHUI/HUI could be described with use of gadoxetate disodium–enhanced MR imaging. We evaluated rV_L/V_L and rHUI/HUI in the patients with segmental heterogeneity of liver function owing to known liver dysfunction, such as portal vein embolization or obstructive jaundice affecting more than one liver subsegment. In this segmental analysis, the same two radiologists mentioned before drew the outlines of the nonaffected liver on gadoxetate disodium–enhanced MR images to obtain rV_L and rL_{20} (Fig 2). The difference between the two methods, calculated as $(rHUI/HUI) - (rV_L/V_L)$, was evaluated.

Statistical Analysis

The mean value and 95% CI for the correlation coefficient between ICG-PDR and feature values (L_{20} and HUI) were determined with a bootstrap method with 2000 bootstrap samples. The bootstrap sample size was determined according to the recommendation that the bootstrap sample size should be 1000 or more to estimate the 95% CI (15).

The stepwise multiple linear regression analysis of the effect of various feature values, including HUI, L_0/S_0, L_{T2*}/S_{T2*}, L_{opp}/L_{in}, S_{opp}/S_{in}, and V_S, on ICG-PDR was performed to evaluate the statistical significance of the various influences, such as iron and fat deposition and splenomegaly, in the correlation between HUI and ICG-PDR. The entrance and exit tolerances for P values of F statistics were specified to be .05 and .1, respectively.

The mean value and 95% CI for $(rHUI/HUI) - (rV_L/V_L)$ were evaluated to determine the significance of the difference between HUI and volumetry in the estimation of segmental liver function.

All statistical analyses were performed with the use of software (Matlab version 7.11, R20010b; MathWorks, Natick, Mass). No overlapping in 95% CIs or P values less than .05 was regarded to indicate a significant difference.

Results

The liver characteristics of all patients obtained in this study are shown in Table 2. The mean value and 95% CI for correlation coefficients between ICG-PDR and feature values were 0.634 (95% CI: 0.629, 0.640) for L_{20} and 0.721 (95% CI: 0.717, 0.726) for HUI (Figs 1, 3, 4).

The stepwise multiple linear regression analysis revealed that HUI and V_S were the factors significantly correlated with ICG-PDR in our study (Table 3). The regression coefficients and the R statistic for a multiple linear regression of HUI and V_S on ICG-PDR (ICG-PDR = $B_0 + B_1HUI + B_2V_S + e$, where B_0, B_1, and B_2 are coefficients and e is a residual in multiple regression) were B_0 of 0.10 (95% CI: 0.07, 0.13), B_1 of 0.12 (95% CI: 0.08, 0.15), B_2 of −0.23 (95% CI: −0.34, −0.11), and R of 0.87 (Fig 5).

The segmental heterogeneity of liver function that affected more than one liver segment was observed in four patients in our study. The liver characteristics of the patients are shown in Table 4. The mean value and 95% CI were 0.18 and 0.01 to 0.34, respectively, for the following equation: $(rHUI/HUI) - (rV_L/V_L)$.

Discussion

The feature value of $V_L[(L_{20}/S_{20}) - 1]$, which may be called the HUI, showed good correlation with ICG-PDR, and the correlation was significantly higher than was the correlation with L_{20}. This result can be explained by two correction factors in addition to the signal intensity of the liver on gadoxetate disodium–enhanced MR images. One

Table 1

Abbreviations Used in This Article

Abbreviation	Definition
CI	Confidence interval
ECF	Extracellular fluid
GRE	Gradient echo
HUI	Hepatocellular uptake index
ICG	Indocyanine green
ICG-PDR	PDR of ICG
L_{in}	Mean signal intensity of the liver on nonenhanced in-phase T1-weighted images
L_{opp}	Mean signal intensity of the liver on nonenhanced opposed-phase T1-weighted images
L_{opp}/L_{in}	Ratio of L_{opp} to L_{in}
L_{T2*}	Mean signal intensity of the liver on nonenhanced T2*-weighted images
L_{T2*}/S_{T2*}	Ratio of L_{T2*} to S_{T2*}
L_{20}	Mean signal intensity of the liver on contrast-enhanced T1-weighted images with fat suppression
L_0	Mean signal intensity of the liver on nonenhanced T1-weighted images with fat suppression
L_{20}/S_{20}	Ratio of L_{20} to S_{20}
L_0/S_0	Ratio of L_0 to S_0
MR	Magnetic resonance
PDR	Plasma disappearance rate
rHUI	Remnant HUI
rHUI/HUI	Ratio of the rHUI to the HUI of the total liver
rL_{20}	Remnant L_{20}
rV_L	Remnant V_L
rV_L/V_L	Ratio of the liver remnant V_L to the total V_L
S_{in}	Mean signal intensity of the spleen on nonenhanced in-phase T1-weighted images
S_{opp}	Mean signal intensity of the spleen on nonenhanced opposed-phase T1-weighted images
S_{opp}/S_{in}	Ratio of S_{opp} to S_{in}
S_{T2*}	Mean signal intensity of the spleen on nonenhanced T2*-weighted images
S_{20}	Mean signal intensity of the spleen on contrast-enhanced T1-weighted images with fat suppression
S_0	Mean signal intensity of the spleen on nonenhanced T1-weighted images with fat suppression
3D	Three-dimensional
V_L	Liver volume
V_S	Spleen volume

Figure 1

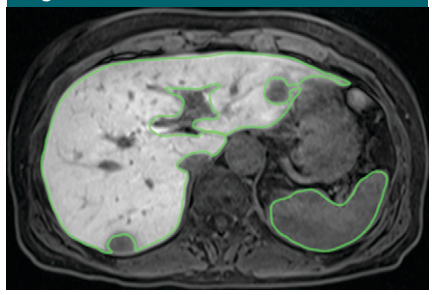

Figure 1: Patient 23. Axial 3D GRE T1-weighted MR image with fat suppression (3.5/1.42; flip angle, 15°) at 20 minutes after gadoxetate disodium administration obtained in a 64-year-old woman with a metastatic liver tumor. The contrast between the liver and spleen is high. Surrounding liver was proved to be normal at surgical resection. HUI is high (1.068 L), consistent with high ICG-PDR (0.207 sec^{-1}). Green lines = outlines of the liver and spleen.

Figure 2

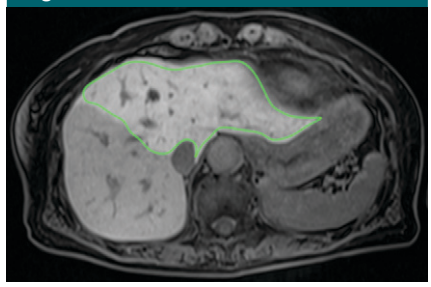

Figure 2: Patient 22. Axial 3D GRE T1-weighted MR image with fat suppression (3.5/1.42; flip angle, 15°) at 20 minutes after gadoxetate disodium administration obtained in a 78-year-old woman with hilar bile duct carcinoma. Portal vein embolization was performed in right branch of portal vein, and the signal intensity in the right hepatic lobe was decreased compared with that in the left hepatic lobe. The rHUI/HUI was 0.43, whereas the rV_L/V_L was 0.32 and lower than the rHUI/HUI. Green lines = outlines used to obtain rHUI and rV_L.

is the ECF contrast enhancement effect of gadoxetate disodium in the liver, approximated by the S_{20}, and the other is the interindividual variation in the V_L.

The local concentration of ICG and gadoxetate disodium taken up by hepatocytes decreases during the development of cirrhosis because of the decrease in hepatocytes and the increase in fibrous tissue (16). In addition, the fibrosis of the liver results in a decrease in the incoming blood flow and restriction of molecular movement in the extravascular space (17), which could be another possible cause of decreased uptake of ICG and gadoxetate disodium by hepatocytes. Although the cause of weak contrast enhancement of gadoxetate disodium in cirrhosis has not been fully clarified, the correlation between contrast enhancement of gadoxetate disodium and the degree of fibrosis has been observed in an animal model (18).

Gadoxetate disodium equilibrates rapidly between the intravascular and extravascular spaces according to the concentration gradient following intravenous administration. Therefore, the contrast enhancement effect of gadoxetate disodium is caused not only by uptake in the hepatocytes but also by its presence in the ECF space (the sum of the intravascular and extravascular spaces) and must be taken into account in the L_{20}. After the gadoxetate disodium reaches equilibrium state in the ECF space (approximately 2 minutes after venous administration), the concentrations of gadoxetate disodium distributing in ECF spaces of the liver and the other organs decrease, in parallel, as a result of renal and hepatic excretion. This phenomenon has been observed on MR images with use of gadoxetate disodium in extrahepatic organs such as the spleen (19). The distribution volume of gadoxetate disodium

Radiology

Table 2

Liver Characteristics of 23 Patients

Patient No.	Degree of Liver Fibrosis	ICG-PDR (sec^{-1})	HUI (L)	V_S (L)	L_{T2*}/S_{T2*}	L_0/S_0	L_{opp}/L_{in}	S_{opp}/S_{in}
1	Liver cirrhosis	0.064	0.425	0.403	0.643	1.434	1.008	0.915
2	Liver cirrhosis	0.071	0.239	0.157	0.736	1.040	0.868	0.939
3	Liver cirrhosis	0.072	0.270	0.115	0.654	1.123	1.035	0.946
4	Liver cirrhosis	0.082	0.203	0.079	1.073	1.068	0.975	0.978
5	Chronic hepatitis	0.083	0.588	0.296	0.712	1.304	0.987	0.898
6	Chronic hepatitis	0.105	0.419	0.136	0.839	1.221	0.859	0.905
7	Liver cirrhosis	0.121	0.365	0.194	0.810	1.102	0.996	0.936
8	Normal liver	0.122	0.787	0.292	1.028	1.229	1.010	0.972
9	Liver cirrhosis	0.130	1.046	0.413	0.631	1.125	0.991	0.911
10	Liver cirrhosis	0.134	0.451	0.122	0.732	1.143	1.003	0.841
11	Normal liver	0.135	0.961	0.150	0.684	1.137	0.957	0.912
12	Liver cirrhosis	0.149	1.165	0.324	0.624	1.632	1.018	0.930
13	Liver cirrhosis	0.149	0.721	0.125	0.560	1.434	0.882	0.902
14	Normal liver	0.152	0.930	0.043	0.769	1.215	1.018	0.926
15	Chronic hepatitis	0.153	0.515	0.148	0.690	1.214	0.967	0.887
16	Liver cirrhosis	0.158	0.464	0.156	0.820	1.167	0.953	0.913
17	Chronic hepatitis	0.179	0.698	0.089	0.840	1.151	0.978	0.888
18	Liver cirrhosis	0.181	0.874	0.099	0.788	1.376	0.981	0.915
19	Chronic hepatitis	0.182	0.407	0.102	1.163	1.108	0.963	0.957
20	Normal liver	0.193	1.296	0.274	0.785	1.286	0.992	0.957
21	Normal liver	0.207	1.068	0.139	0.890	1.040	1.013	0.898
22	Normal liver	0.215	1.001	0.077	0.984	1.464	0.977	0.872
23	Chronic hepatitis	0.267	1.475	0.108	0.836	1.049	0.960	0.913

Figure 3

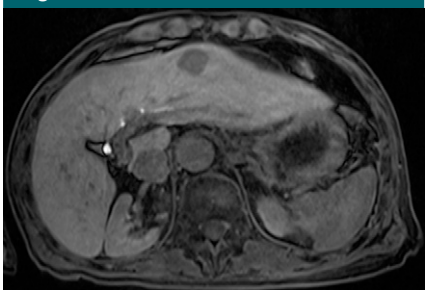

Figure 3: **Patient 4.** Axial 3D GRE T1-weighted MR image with fat suppression (3.5/1.42; flip angle, 15°) at 20 minutes after gadoxetate disodium administration obtained in a 73-year-old man with hepatocellular carcinoma. The contrast between the liver and spleen is low. Surrounding liver was proved to be cirrhotic at surgical resection. HUI was low (0.203 L) consistent with a low ICG-PDR (0.082 sec^{-1}).

Figure 4

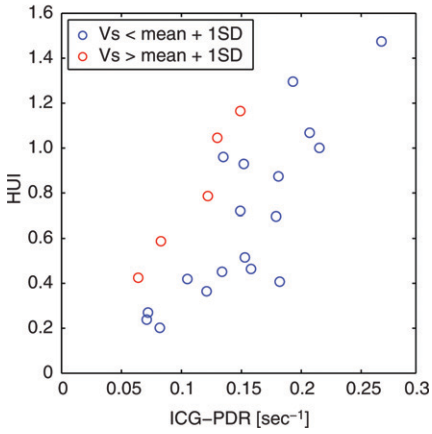

Figure 4: Correlation of HUI and ICG-PDR. Blue circles = patients without splenomegaly *(Vs < mean + 1 SD)*, red circles = patients with splenomegaly *(Vs > mean + 1 SD)*. *SD* = standard deviation.

Table 3

Stepwise Multiple Linear Regression Analysis of Various Factors for Effect on ICG-PDR

Variable	Coefficient	*P* Value
HUI	0.116	<.01
V_S	−0.229	<.01
L_{T2*}/S_{T2*}	0.075	.06
L_0/S_0	−0.016	.69
L_{opp}/L_{in}	−0.001	.99
S_{opp}/S_{in}	−0.152	.42

in the ECF correlates closely with the ECF volume after the equilibrium is reached, and the ECF volume is similar between the liver and spleen in normal liver and spleen (20). Therefore, the parameter $(L_{20}/S_{20}) - 1$ could serve as an index for the hepatocellular contrast enhancement effect corrected by the ECF contrast enhancement effect approximated by the signal intensity of the spleen.

The relationship between the distribution volume and the degree of liver fibrosis is controversial (21,22). Van Beers et al (21) reported that distribution volume of the liver would not be affected by the degree of liver fibrosis. In contrast, Hagiwara et al (22) demonstrated a significant increase in distribution volume between normal liver and liver with fibrosis; however, the increase of distribution volume owing to liver fibrosis compared with normal liver has been reported as 10%. On the other hand, the relaxivity of gadoxetate disodium in ECF space (8.7 L/mmol · sec)

Figure 5

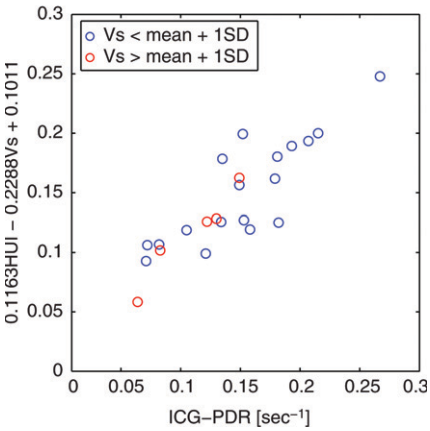

Figure 5: Regression analysis of HUI and V_S on ICG-PDR. Blue circles = patients without splenomegaly *(Vs < mean + 1 SD)*, red circles = patients with splenomegaly *(Vs > mean + 1 SD)*. *SD* = standard deviation.

Table 4

Characteristics of Four Patients with Segmental Heterogeneity of Liver Function

Patient No.	Affected Segment*	Cause	Difference between Methods†
4	V–VIII	Obstructive jaundice	0.428
8	VIII	Obstructive jaundice	0.120
13	V–VIII	Obstructive jaundice	0.068
22	V–VIII	Portal vein embolization	0.083

* The Couinaud system was used to designate liver segments.

† The difference was calculated as follows: rHUI/HUI − rV_L/V_L.

is about one-half compared with that in hepatocytes (16.6 L/mmol · sec), related to differences in microviscosity (23). Therefore, the influence of various distribution volumes in the liver according to liver fibrosis could be less than 10% and negligible in the signal intensity of the liver at 20 minutes after gadoxetate disodium administration (L_{20}).

On the other hand, our results showed that the V_S could be a significant factor that affects the correlation between HUI and ICG-PDR. This can be explained by the effect of splenomegaly due to portal hypertension in the splenic ECF volume. There have been several reports that show the hyperplasia of the red pulp and the decrease of the vascular space density in the spleen during the development of splenomegaly due to portal hypertension (24). The increase of splenic hematocrit level due to congestion may decrease the ECF space density in the spleen, as has been suggested in the animal model with portal hypertension (25). Therefore, the decrease of ECF space density correlating with splenomegaly (increase in V_S) may lead to the weak contrast enhancement of the spleen after the equilibrium point (decrease in S_{20}) and result in an increase of HUI, $V_L[(L_{20}/S_{20}) - 1]$, on gadoxetate disodium–enhanced MR images; however, this hypothesis must be confirmed with further investigation. In the future, a more accurate index derived from HUI to estimate liver function, taking into account the volume of the spleen, could be possible with use of gadoxetate disodium–enhanced MR imaging.

If the parameter $(L_{20}/S_{20}) - 1$ was analogous to the concentration of gadoxetate disodium taken up by hepatocytes, the total amount of gadoxetate disodium taken up by hepatocytes that can correlate with ICG-PDR would be found by the volume integration of $(L_{20}/S_{20}) - 1$. The similar idea has been proposed in the relationship with histologic evaluation of liver fibrosis. It was shown by Hashimoto and Watanabe (26) that ICG-PDR was proportional to the total hepatic parenchymal cell volume, determined as the histologic parenchymal cell volume ratio multiplied by the liver volume obtained from computed tomography. The liver volume differs, depending on not only the severity of chronic liver disease but also the physical constitution (27), and the total hepatic parenchymal cell volume differs individually. Thus, a correction for liver volume is necessary for estimation of ICG-PDR from the hepatobiliary contrast enhancement of gadoxetate disodium in the liver.

The signal intensity of the liver and the spleen on gadoxetate disodium–enhanced MR images can be affected by various factors, including liver function but also the difference of tissue specific relaxation time and the iron and/or fat deposition. However, our multiple regression analysis revealed that these effects were not significant in the correlation between HUI and ICG-PDR. This factor could be explained by the use of a very-short echo time with the 3D GRE sequence in the measurement of HUI in this study. The shorter the echo time is, the less a T2*-weighted and the more a T1-weighted image could be obtained. Thus, correlation of the contrast enhancement effect in the liver to liver function is much greater than the correlation of the contrast enhancement effect of other factors that affect the signal intensity of the liver and the spleen in gadoxetate disodium–enhanced MR imaging.

The uptake of ICG and gadoxetate disodium into hepatocytes reflects not only the hepatic cell function but also the hepatic blood flow (28); therefore the ICG-PDR and HUI might show a discrepancy from the galactosyl–human serum albumin scintigraphy result, which is less affected by the hepatic blood flow, in some circulation disorders such as portosystemic shunt, increased plasma volume, and decreased cardiac output.

The V_L and a quantitative liver function test, such as the ICG clearance test, have been reported to be significant predictors of postoperative liver failure and mortality (1,29). However, our results showed that the segmental liver reserve estimated with volumetry (rV_L/V_L) was significantly smaller than that estimated with HUI (rHUI/HUI). Therefore, with volumetry, underestimation of the segmental liver reserve could occur because the heterogeneity of the liver function could not be taken into account. Because the HUI can correlate with ICG-PDR very well and it can be determined directly from the volume and the signal intensity of a region of interest in the liver, the quantitative estimation of total and segmental liver function may be feasible. Therefore, gadoxetate disodium–enhanced MR imaging has

the potential to provide the required information for the diagnosis and treatment of liver diseases with one examination, which can be essential to early detection and treatment.

Our study had several limitations. First, the study population was small, and further prospective validation with a large population, especially on segmental variation in liver function, is needed. Second, nonenhanced images were not used with our eventual model; however, the effect of the difference in the signal intensity between the liver and the spleen on nonenhanced images was not significant. Therefore, HUI can be more convenient to apply for clinical practice than use of changes in signal intensity between nonenhanced and contrast-enhanced images.

In conclusion, the liver function correlating with ICG-PDR can be estimated quantitatively from the signal intensities and the volumes of the liver and spleen on gadoxetate disodium–enhanced MR images, which may improve the estimation of the segmental liver reserve.

Acknowledgments: We thank Daisuke Komatsu, MD, and Mai Maruyama, MD, both from Department of Radiology, Shinsu University School of Medicine, Matsumoto, Japan, for drawing outlines on MR images.

Disclosures of Potential Conflicts of Interest: A.Y. No potential conflicts of interest to disclose. **T.H.** No potential conflicts of interest to disclose. **F.L.** Financial activities related to the present article: none to disclose. Financial activities not related to the present article: institution received grants from Riverain Medical, and institution has patents and received royalties for CAD technologies developed in the University of Chicago that have been licensed to R2 Technology (Hologic), Deus Technologies, Riverain Medical, Mitsubishi Space Software, Median Technologies, GE Healthcare, and Toshiba. Other relationships: none to disclose. **Y.F.** No potential conflicts of interest to disclose. **K.U.** No potential conflicts of interest to disclose. **M.K.** No potential conflicts of interest to disclose. **K.D.** No potential conflicts of interest to disclose.

References

1. Seyama Y, Kokudo N. Assessment of liver function for safe hepatic resection. Hepatol Res 2009;39(2):107–116.
2. Sakka SG. Assessing liver function. Curr Opin Crit Care 2007;13(2):207–214.
3. Reimer P, Schneider G, Schima W. Hepatobiliary contrast agents for contrast-enhanced MRI of the liver: properties, clinical development and applications. Eur Radiol 2004;14(4):559–578.
4. Clément O, Mühler A, Vexler V, Berthezène Y, Brasch RC. Gadolinium-ethoxybenzyl-DTPA, a new liver-specific magnetic resonance contrast agent: kinetic and enhancement patterns in normal and cholestatic rats. Invest Radiol 1992;27(8):612–619.
5. Meier PJ, Eckhardt U, Schroeder A, Hagenbuch B, Stieger B. Substrate specificity of sinusoidal bile acid and organic anion uptake systems in rat and human liver. Hepatology 1997;26(6):1667–1677.
6. Shimizu J, Dono K, Gotoh M, et al. Evaluation of regional liver function by gadolinium-EOB-DTPA-enhanced MR imaging. Dig Dis Sci 1999;44(7):1330–1337.
7. Schmitz SA, Mühler A, Wagner S, Wolf KJ. Functional hepatobiliary imaging with gadolinium-EOB-DTPA: a comparison of magnetic resonance imaging and 153gadolinium-EOB-DTPA scintigraphy in rats. Invest Radiol 1996;31(3):154–160.
8. Kim T, Murakami T, Hasuike Y, et al. Experimental hepatic dysfunction: evaluation by MRI with Gd-EOB-DTPA. J Magn Reson Imaging 1997;7(4):683–688.
9. Nilsson H, Nordell A, Vargas R, Douglas L, Jonas E, Blomqvist L. Assessment of hepatic extraction fraction and input relative blood flow using dynamic hepatocyte-specific contrast-enhanced MRI. J Magn Reson Imaging 2009;29(6):1323–1331.
10. Ryeom HK, Kim SH, Kim JY, et al. Quantitative evaluation of liver function with MRI using Gd-EOB-DTPA. Korean J Radiol 2004;5(4):231–239.
11. Motosugi U, Ichikawa T, Tominaga L, et al. Delay before the hepatocyte phase of Gd-EOB-DTPA-enhanced MR imaging: is it possible to shorten the examination time? Eur Radiol 2009;19(11):2623–2629.
12. Moody FG, Rikkers LF, Aldrete JS. Estimation of the functional reserve of human liver. Ann Surg 1974;180(4):592–598.
13. Gandon Y, Olivié D, Guyader D, et al. Noninvasive assessment of hepatic iron stores by MRI. Lancet 2004;363(9406):357–362.
14. Rinella ME, McCarthy R, Thakrar K, et al. Dual-echo, chemical shift gradient-echo magnetic resonance imaging to quantify hepatic steatosis: implications for living liver donation. Liver Transpl 2003;9(8):851–856.
15. Martinez W, Martinez A. Bootstrap methods. In: Computational statistics handbook with MATLAB. 2nd ed. Boca Raton, Fla: Chapman & Hall/CRC, 2007; 256–262.
16. Malhi H, Gores GJ. Cellular and molecular mechanisms of liver injury. Gastroenterology 2008;134(6):1641–1654.
17. Van Beers BE, Materne R, Annet L, et al. Capillarization of the sinusoids in liver fibrosis: noninvasive assessment with contrast-enhanced MRI in the rabbit. Magn Reson Med 2003;49(4):692–699.
18. Tsuda N, Okada M, Murakami T. New proposal for the staging of nonalcoholic steatohepatitis: evaluation of liver fibrosis on Gd-EOB-DTPA-enhanced MRI. Eur J Radiol 2010;73(1):137–142.
19. Runge VM. A comparison of two MR hepatobiliary gadolinium chelates: Gd-BOPTA and Gd-EOB-DTPA. J Comput Assist Tomogr 1998;22(4):643–650.
20. Kötz B, West C, Saleem A, Jones T, Price P. Blood flow and Vd (water): both biomarkers required for interpreting the effects of vascular targeting agents on tumor and normal tissue. Mol Cancer Ther 2009;8(2):303–309.
21. Van Beers BE, Leconte I, Materne R, Smith AM, Jamart J, Horsmans Y. Hepatic perfusion parameters in chronic liver disease: dynamic CT measurements correlated with disease severity. AJR Am J Roentgenol 2001;176(3):667–673.
22. Hagiwara M, Rusinek H, Lee VS, et al. Advanced liver fibrosis: diagnosis with 3D whole-liver perfusion MR imaging—initial experience. Radiology 2008;246(3):926–934.
23. Schuhmann-Giampieri G, Schmitt-Willich H, Press WR, Negishi C, Weinmann HJ, Speck U. Preclinical evaluation of Gd-EOB-DTPA as a contrast agent in MR imaging of the hepatobiliary system. Radiology 1992;183(1):59–64.
24. Cavalli G, Re G, Casali AM. Red pulp arterial terminals in congestive splenomegaly. A morphometric study. Pathol Res Pract 1984;178(6):590–594.
25. Kaufman S, Levasseur J. Effect of portal hypertension on splenic blood flow, intraplenic extravasation and systemic blood pressure. Am J Physiol Regul Integr Comp Physiol 2003;284(6):R1580–R1585.
26. Hashimoto M, Watanabe G. Hepatic parenchymal cell volume and the indocyanine green tolerance test. J Surg Res 2000;92(2):222–227.
27. Zhou XP, Lu T, Wei YG, Chen XZ. Liver volume variation in patients with virus-induced cirrhosis: findings on MDCT. AJR Am J Roentgenol 2007;189(3):W153–W159.
28. Nanashima A, Yamaguchi H, Shibasaki S, et al. Relationship between indocyanine green test and technetium-99m galactosyl serum albumin scintigraphy in patients scheduled for hepatectomy: clinical evaluation and patient outcome. Hepatol Res 2004;28(4):184–190.
29. Suda K, Ohtsuka M, Ambiru S, et al. Risk factors of liver dysfunction after extended hepatic resection in biliary tract malignancies. Am J Surg 2009;197(6):752–758.